IEEE Access
Multidisciplinary | Rapid Review | Open Access Journal

Received June 2, 2019, accepted July 6, 2019, date of publication July 30, 2019, date of current version August 19, 2019.

Digital Object Identifier 10.1109/ACCESS.2019.2932077

A Reinforced Blind Color Image Watermarking Scheme Based on Schur Decomposition

LING-YUAN HSU[1] AND HWAI-TSU HU[2], (Member, IEEE)
[1]Department of Information Management, St. Mary's Junior College of Medicine, Nursing and Management, I-Lan 26647, Taiwan
[2]Department of Electronic Engineering, National ILan University, I-Lan 26047, Taiwan

Corresponding author: Hwai-Tsu Hu (hthu@mail.niu.edu.tw)

This work was supported by the Ministry of Science and Technology, Taiwan, ROC, under Grant MOST 107-2221-E-562-002 and Grant 106-2221-E-197-025.

ABSTRACT In this paper, the deficiency of Schur decomposition (SD) for image watermarking has been comprehensively investigated. A remedial scheme is developed not only to fix the existing problems but also to reinforce the performance in robustness and imperceptibility. This scheme starts with partitioning the host image into non-overlapping blocks of 4×4 pixels and then applying SD to each block individually. Level shifting serves as a controlling gauge for embedding strength. The use of intentional perturbation prevents nil orthonormal vectors derived from zero eigenvalues. The dominant vector is identified by analyzing the entire Schur matrix instead of just diagonal elements. To achieve effective watermark embedding and extraction, the orthonormality of the acquired unitary matrix ought to be preserved while the resulting distortion can be compensated via the systematic modification of the Schur matrix. Finally, a recursive regulation guarantees the retrieval of watermark bits. Experiment results indicate that the proposed scheme is free of errors in the absence of attacks and can withstand a variety of image processing attacks as well. Moreover, the inclusion of distortion compensation contributes an improvement of 2.47 dB in terms of peak signal-to-noise ratio. In comparison with previous SD-based schemes, the proposed one exhibits superior robustness and imperceptibility while operating at the same payload capacity.

INDEX TERMS Blind color image watermarking, Schur decomposition, orthonormal reconstruction, watermark retrieval assurance, distortion compensation.

I. INTRODUCTION

With the rapid development of network and computer technology, a verity of digital multimedia (such as images, audios and videos) are widely spread on the internet nowadays. Great convenience has been brought to daily work and life. People obtain multimedia information much easier and faster ever than before. However, multimedia data also have the characteristics of fast propagation and easy modification. They can be easily tampered and redistributed. Internet piracy and propriety infringement become more and more frequent. The issue of multimedia security has raised the concern of general public and also attracted the attention of many researchers [1]. Digital watermarking is a promising technique developed to deal with this issue. It provides an effective solution to prevent the theft or unauthorized use of intellectual property.

Digital watermarking techniques can be categorized into three types (i.e., non-blind, semi blind and blind) based on the materials participating in watermark extraction. For non-blind watermarking techniques, the watermark extraction requires the presence of the original source [2]. Semi-blind watermarking needs side information to recover the embedded watermark [3]. Blind watermarking uses neither the original source nor watermark in the extraction. Compared with the non-blind watermarking, blind watermarking is generally preferable in practical applications since the original source may not always be accessible.

Blind image watermarking techniques can be classified into spatial or transform domains in accordance with the object where the watermark is embedded. Spatial domain techniques are easy to implement with low complexity, but less preferred since they are not robust to image processing manipulations such as filtering and lossy compression. By contrast, the transform domain approach provides superior robustness against malicious attacks, as the watermarks

The associate editor coordinating the review of this manuscript and approving it for publication was Wei Liu.

can be hidden inside transform coefficients with stronger noise tolerance. Commonly used transform domain techniques include discrete Fourier transform (DFT) [4]–[6], discrete cosine transform (DCT) [7]–[12], discrete wavelet transform (DWT) [6], [13]–[15], and matrix factorization (such as singular value decomposition (SVD) [16]–[19], QR decomposition [20], [21], LU decomposition [22], [23], and Schur decomposition (SD) [24]–[26]).

For two-dimensional image analysis, matrix factorization is considered an effective mean to decompose an image to physically meaningful data. The developed techniques were widely applied to image watermarking. It has been demonstrated in the literature [16]–[18], [25] that SVD-based blind image watermarking provided excellent efficiency. The main idea is to perform SVD over the partitioned blocks of a cover image, and then modify pivotal elements in factorized matrixes while embedding the watermark. However, SVD requires rather sophisticated computation in comparison with SD. In fact, SD represents an intermediate step in SVD decomposition. A SD-based image watermarking scheme not only demands less computation but renders comparable robustness in a similar manner as the SVD does [24]–[26]. In practical computation, SVD demands approximately $11N^3$ flops for a matrix of size $N \times N$, whereas SD requires approximately $8N^3/3$ flops [27], [28], indicating that SD requires two thirds fewer operations than SVD does. For SD-based image watermarking, a commonly used block size is 4×4, i.e., $N = 4$. Advantages gained from a small N like $N = 4$ manifests not only in computational efficiency but also in the amount of embeddable watermark bits in a host image.

A number of SD-based schemes have been proposed to facilitate binary embedding in images. Su *et al.* [26] introduced a primitive SD-based color image watermarking scheme (hereby designated as PSD for short), which embeds the watermarks by manipulating the relationship of two elements in the first column vector of the unitary matrix derived by SD. Liu *et al.* [29] proposed another SD-based scheme (designated as LSD), which modifies the largest eigenvalue in the Schur matrix. In a subsequent study, Su and Chen [24] made an improvement for the PSD scheme. The resultant scheme (designated as ISD) embedded the watermark via the inequality correlation between the second and third elements drawn from the column vector corresponding to the largest eigenvalue. Recently, Su *et al.* [30] proposed an approximate SD-based spatial domain watermarking scheme. This scheme (herein referred to as ASD) calculates the approximate maximum eigenvalue of SD to achieve low computational complexity. Although the foregoing SD-based watermarking schemes achieved satisfactory performance in the imperceptibility, robustness, capacity and computational complexity, they suffered an innate drawback that the watermark cannot be thoroughly recovered even in the absence of attacks. Hence a reinforced SD scheme (named as RSD hereby) is proposed to rectify the deficiency of previous SD-based watermark techniques.

The remaining sections of this paper are organized as follows. Section II discusses techniques relevant to the basic properties of SD. Details of the proposed blind image watermark embedding and extraction procedures are elucidated in Section III. Section IV presents the experiment results and the comparisons with other related schemes in terms of imperceptibility and robustness. Section V summarizes the contributions of this paper.

II. RELEVANT TECHNIQUES

In this section, we first review the matrix operations of SD. The relevant techniques then serve as the groundwork in the development of a reinforced blind watermarking scheme.

A. SCHUR DECOMPOSITION (SD)

The SD factorizes a real matrix $\mathbf{A}$(presumably of size 4×4) as a product of

$$\begin{aligned}\mathbf{A} &= \mathbf{U}\mathbf{T}\mathbf{U}^T \\ &= [\mathbf{u}_1\ \mathbf{u}_2\ \mathbf{u}_3\ \mathbf{u}_4] \begin{bmatrix} t_{11} & t_{12} & t_{13} & t_{14} \\ t_{21} & t_{22} & t_{23} & t_{24} \\ 0 & t_{32} & t_{33} & t_{34} \\ 0 & 0 & t_{43} & t_{44} \end{bmatrix} \begin{bmatrix} \mathbf{u}_1^T \\ \mathbf{u}_2^T \\ \mathbf{u}_3^T \\ \mathbf{u}_4^T \end{bmatrix}, \end{aligned} \quad (1)$$

where $\mathbf{U}$ is a unitary matrix consisting of orthonormal vectors $\mathbf{u}_k's$, and $\mathbf{U}^T$ stands for the transposed $\mathbf{U}$. Here the Schur matrix $\mathbf{T}$ is represented in a *real* Schur form, which is essentially an upper triangular matrix with the diagonal filled by either single elements for real eigenvalues or 2-by-2 blocks for complex eigenvalues. Thus, the elements t_{21}, t_{32}, and t_{43} in $\mathbf{T}$ may be nonzero whenever complex eigenvalues emerge.

B. BLIND WATERMARKING BASED ON SD

While using SD to embed a watermark bit w_b into an image of size 4×4 , Su *et al.* [24] suggested to modify the magnitudes of the 2nd and 3rd elements in the column vector $\mathbf{u}_k$ that corresponds to the largest eigenvalue, said t_{kk}.

$$\begin{cases} \hat{u}_{2k} = \text{sign}(u_{2k}) \times \left(\dfrac{|u_{2k}| + |u_{3k}|}{2} + (-1)^{w_b+1}\, \alpha\beta \right) \\ \hat{u}_{3k} = \text{sign}(u_{3k}) \times \left(\dfrac{|u_{2k}| + |u_{3k}|}{2} + (-1)^{w_b}\ \alpha(1-\beta) \right) \end{cases} \quad (2)$$

where $\text{sign}(\cdot)$ and $|\cdot|$ symbolize the sign and absolute functions, respectively. The variable α denotes a threshold value and β represents an embedding factor. Substituting $\hat{\mathbf{u}}_k$ for $\mathbf{u}_k$ in Eq. (1) leads to a watermarked matrix $\hat{\mathbf{A}}$. The watermark bit can be later retrieved by examining whether the magnitude of the 2nd elements in the retrieved $\hat{\mathbf{u}}_k$, termed $\hat{\mathbf{u}}_k'$ for the sake of differentiation, is greater than that of the 3rd element in the same vector.

$$\hat{w}_b' = \begin{cases} 1, & \text{if } |\hat{u}_{2k}'| \geq |\hat{u}_{3k}'|\,; \\ 0, & \text{otherwise.} \end{cases} \quad (3)$$

Here the prime sign implicates that the retrieval is from a recomposed matrix $\hat{\mathbf{A}}$ rather than from Eq. (2). Most often,

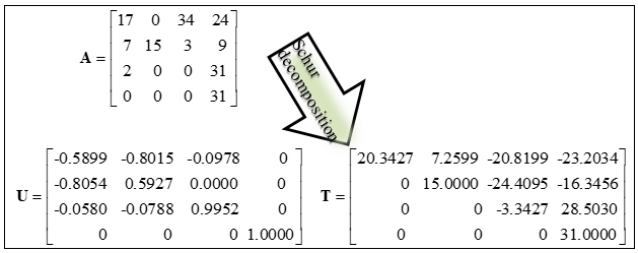

FIGURE 1. Illustrative example: The largest eigenvalue may not stand at the leading position.

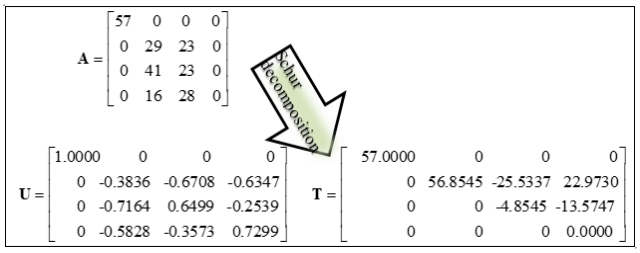

FIGURE 2. Illustrative example: The vector associated with the largest eigenvalue may not be the dominant vector.

the largest eigenvalue happens at the first position, i.e., $k = 1$. Thus, the focus is usually placed on u_{21} and u_{31} [26].

Our experimental results indicate that the use of the above-mentioned approach cannot always come up with perfect watermark extraction. The problem lies in the oversimplification of the SD structure in manifold. First, the largest eigenvalue may not be at the leading position. Figure 1 demonstrates a typical example. Second, the vector associated with the largest eigenvalue may not be the predominant vector in $\mathbf{U}$. Figure 2 illustrates such a situation. In this particular case, we argue that the column vector associated with the second eigenvalue is more suitable for performing watermark embedding, as its influence on the image block is larger than the first column. Third, there is no guarantee that the $\hat{u}'_{2k}$ and $\hat{u}'_{3k}$ recovered from a recomposed matrix can still maintain the expected relationship as specified in Eqs. (2) and (3). Figure 3 shows an example of SD, wherein the use of Eq. (2) for embedding a binary bit $w_b = 0$ into matrix $\mathbf{U}$ renders $\hat{u}_{21} = 0.4995$ and $\hat{u}_{31} = 0.5045$, respectively. During watermark extraction, the retrieved $\hat{u}'_{21}$ and $\hat{u}'_{31}$ are 0.5026 and 0.5023 respectively, suggesting that $\hat{w}'_b = 1$ instead. Fourth, the saturation and round-off errors may cause unexpected outcomes while converting the resulting elements to unsigned 8-bit pixel values. Figure 4 exemplifies one such case, where the embedding of $w_b = 0$ into matrix $\mathbf{U}$ leads to $\hat{u}_{21} = 0.4441$ and $\hat{u}_{31} = 0.4491$. Let $\hat{\mathbf{A}}_{\text{unit8}} = \{f_{\text{unit8}}(\hat{a}_{ij})\}_{4\times4}$ denote the resultant matrix after Schur reconstruction and unsigned 8-bit integer casting. $f_{\text{uint8}}(\cdot)$ represents an unsigned 8-bit integer casting function defined as

$$f_{\text{uint8}}(x) = \begin{cases} 0, & \text{if} x \le 0; \\ \lfloor x + 0.5 \rfloor, & \text{if} 0 < x < 255; \\ 255, & \text{if} x \ge 255, \end{cases} \tag{4}$$

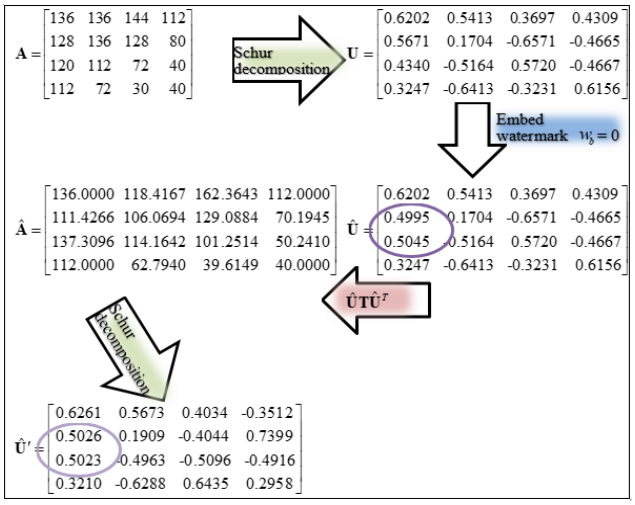

FIGURE 3. Illustrative example: The recovered u_{2k} and u_{3k} may not maintain a desired inequality relationship.

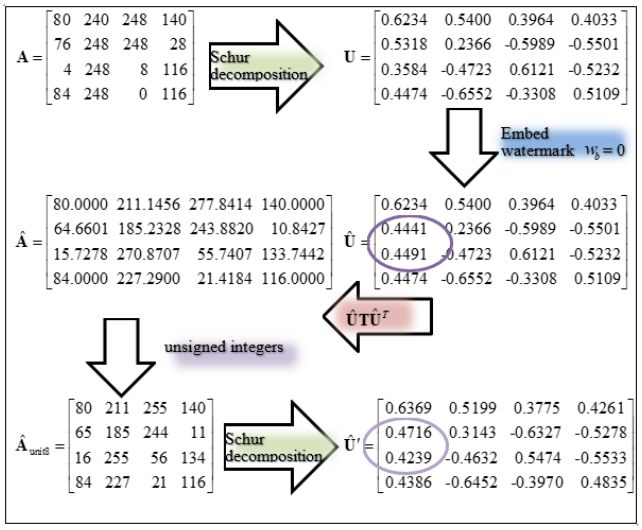

FIGURE 4. Illustrative example: The effect due to the saturation and round-off errors.

with $\lfloor \cdot \rfloor$ being the floor function. In the example shown in Fig. 4, the recomposed pixel values $\hat{a}'_{13}(= 277.8414)$ and $\hat{a}'_{32}(= 270.8707)$ are both recast as 255. Via the SD-based watermarking process, the obtained $\hat{u}'_{21}$ and $\hat{u}'_{31}$ are 0.4716 and 0.4239, respectively. According to Eq. (3), the binary bit acquired from $\hat{\mathbf{u}}'_1$ is $\hat{w}'_b = 1$, which disagrees with the intended one. From the above discussion, it appears that the use of SD for watermarking is feasible only if we can resolve all the aforementioned problems.

III. PROPOSED BLIND WATERMARKING SCHEME

In this section we present a reinforced SD-based (RSD) watermarking scheme to not only remedy the existing problems but empower the SD with additional functionalities such as embedding strength control and distortion compensation. Figure 5 depicts the embedding procedure of the proposed

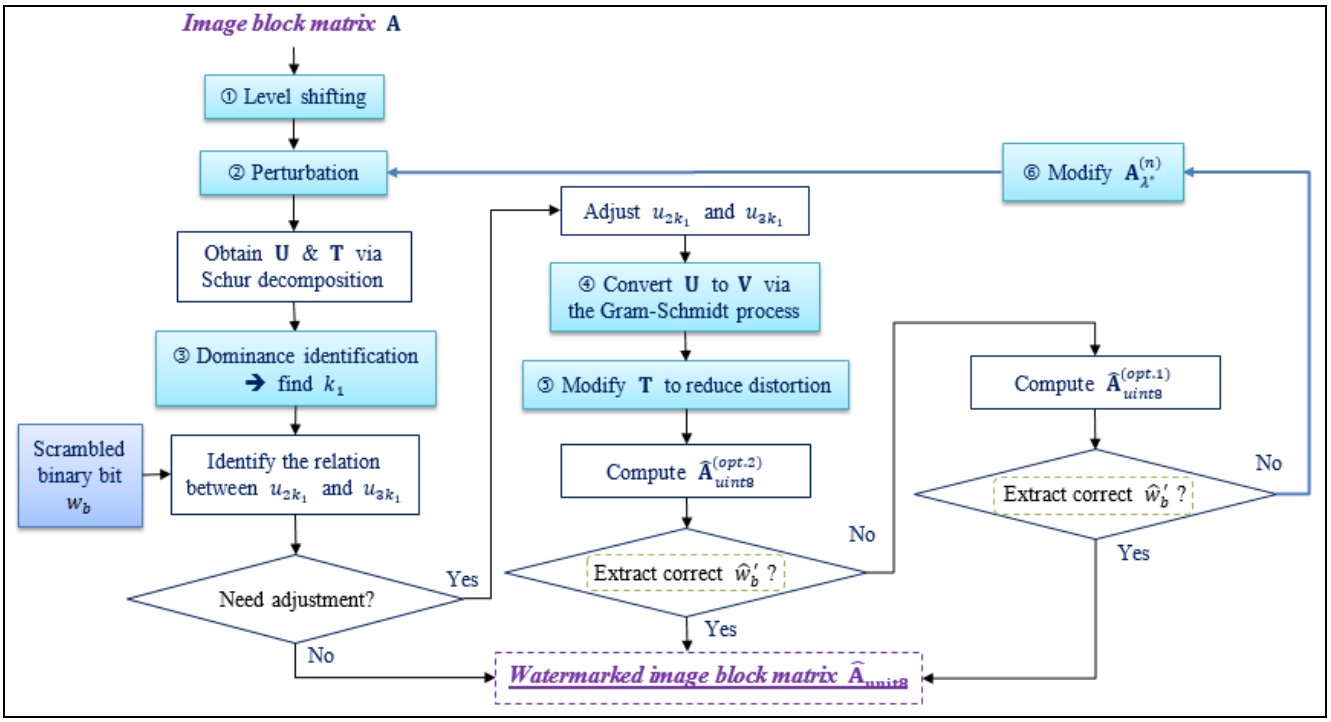

FIGURE 5. Embedding procedure of the reinforced SD-based watermarking scheme.

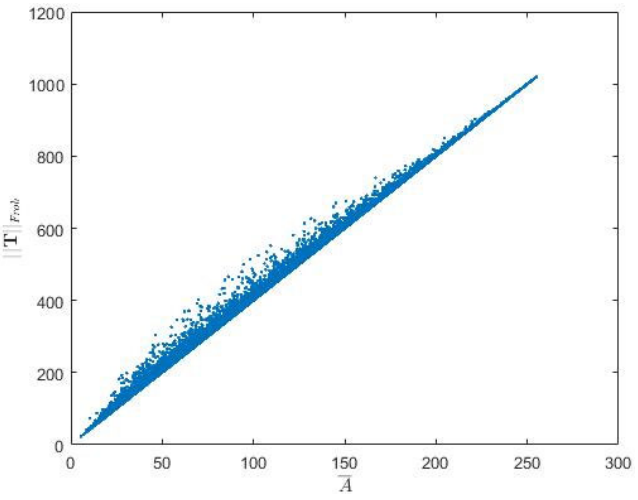

FIGURE 6. Sampling distribution between $\|\mathbf{T}\|_{Frob}$ and $\bar{A}$ based on data drawn from the "*Lena*" image.

RSD scheme. The steps for embedding a watermark bit into a block matrix of size 4 × 4 consist of (1) level shifting, (2) intentional perturbation, (3) dominance identification, (4) orthonormal reconstruction, (5) distortion compensation, and (6) recursive regulation.

A. LEVEL SHIFTING

Through SD a matrix can be expressed as a combination of image planes $\left\{\mathbf{u}_i\mathbf{u}_j^T\right\}$, each of which is scaled by a factor t_{ij} as follows:

$$\mathbf{A} = [\mathbf{u}_1\ \mathbf{u}_2\ \mathbf{u}_3\ \mathbf{u}_4]\begin{bmatrix} t_{11} & t_{12} & t_{13} & t_{14} \\ t_{21} & t_{22} & t_{23} & t_{24} \\ 0 & t_{32} & t_{33} & t_{34} \\ 0 & 0 & t_{43} & t_{44} \end{bmatrix}\begin{bmatrix} \mathbf{u}_1^T \\ \mathbf{u}_2^T \\ \mathbf{u}_3^T \\ \mathbf{u}_4^T \end{bmatrix}$$
$$= \sum_{i=1}^{4}\sum_{j=i}^{4} t_{ij}\mathbf{u}_i\mathbf{u}_j^T + \left(t_{21}\mathbf{u}_2\mathbf{u}_1^T + t_{32}\mathbf{u}_3\mathbf{u}_2^T + t_{43}\mathbf{u}_4\mathbf{u}_3^T\right) \quad (5)$$

The embedding strength, as characterized by the extent of signal alteration, is therefore proportional to the magnitude variations of the elements in **T**. For a matrix deduced from an image with non-negative pixel values, the elements in **T** incline to exhibit large magnitudes whenever the pixel intensity is high. Figure 6 depicts the sampling distribution between the Frobenius norm of matrix **T** (termed $\|\mathbf{T}\|_{Frob}$) and the average intensity of matrix **A**(termed $\bar{A}$) drawn from a classic image "Lena".

$$\|\mathbf{T}\|_{Frob} = \left(\sum_{i=1}^{4}\sum_{j=1}^{4} t_{ij}^2\right)^{1/2}; \quad (6)$$

$$\bar{A} = \frac{1}{16}\sum_{i=1}^{4}\sum_{j=1}^{4} a_{ij}. \quad (7)$$

The plot in Fig. 6 suggests that the elements in **T** generally vary proportionally to $\bar{A}$. As a result, the embedding strength is usually strong for bright image blocks but weak for dark image blocks. To amend this drawback, we propose shifting

the intensity level to a designated value λ before actually carrying out the SD watermarking.

$$\mathbf{A}_\lambda = \mathbf{A} + \left(\lambda - \bar{A}\right) \begin{bmatrix} 1 & 1 & 1 & 1 \\ 1 & 1 & 1 & 1 \\ 1 & 1 & 1 & 1 \\ 1 & 1 & 1 & 1 \end{bmatrix} = \mathbf{U}_\lambda \mathbf{T}_\lambda \mathbf{U}_\lambda^T, \quad (8)$$

where $\mathbf{U}_\lambda$ and $\mathbf{T}_\lambda$ are the unitary and upper triangular matrices resulting from the SD of $\mathbf{A}_\lambda$. Thus, the manipulation in $\mathbf{U}_\lambda$ is more likely to render a commensurate degree of signal alteration regardless of the pixel intensity.

B. INTENTIONAL PERTURBATION

While using the SD to decompose matrix $\mathbf{A}_\lambda$, one may also encounter an awkward condition that the eigenvalues turn out to be all zeros. In such a condition, some of the vectors in $\mathbf{U}_\lambda$ are problematic since they are derived from zero eigenvalues. To prevent this kind of predicament, we deliberately add a small amount of perturbation noise to $\mathbf{A}_\lambda$, i.e.,

$$\mathbf{A}_{\lambda^*} = \mathbf{A} + \left(\lambda - \bar{A}\right) \mathbf{1}_{4\times 4} + \mathbf{E}_{4\times 4}, \quad (9)$$

where $\mathbf{1}_{4\times4}$ is a matrix with all elements being ones. $\mathbf{E}_{4\times4} = \{e_{ij}\}_{4\times4}$ contains numbers randomly distributed from -0.5 to 0.5. The additive noise is merely for the purpose of facilitating the SD watermarking, the effect due to the noise will be removed when we recast the matrix elements as 8-bit unsigned integers.

C. DOMINANCE IDENTIFICATION

In the sequel, we assume that the SD is applied to $\mathbf{A}_{\lambda^*}$ and omit the subscript label λ^* alongside with $\mathbf{U}$ and $\mathbf{T}$ for the sake of conciseness. Eq. (5) reflects a fact that the alteration in an arbitrary vector, said $\mathbf{u}_k$, will be amplified by the interrelated elements $t'_{ik}s$ and $t'_{kj}s$ in $\mathbf{T}$. In other words, the element t_{ij} not located in the diagonal may considerably contribute to the matrix formation, suggesting that we shall take into account of the off-diagonal elements in $\mathbf{T}$, i.e. vector $\mathbf{u}_k$, we draw out the components pertaining to $\mathbf{u}_k$ and compute the Frobenius norm, termed η_k, as the following:

$$\begin{aligned} \eta_k &= \left\| \sum_{i=1}^{4} \left(t_{ik}\mathbf{u}_i\mathbf{u}_k^T + t_{ki}\mathbf{u}_k\mathbf{u}_i^T \right) \right\|_{Frob} \\ &= \left(trace\left(\left(\sum_{i=1}^{4} \left(t_{ik}\mathbf{u}_i\mathbf{u}_k^T + t_{ki}\mathbf{u}_k\mathbf{u}_i^T \right) \right) \right.\right. \\ &\quad \left.\left. \times \left(\sum_{i=1}^{4} \left(t_{ik}\mathbf{u}_i\mathbf{u}_k^T + t_{ki}\mathbf{u}_k\mathbf{u}_i^T \right) \right)^T \right) \right)^{1/2} \\ &= \left(\sum_{i=1}^{4} \left(t_{ik}^2 + t_{ki}^2 \right) - t_{kk}^2 \right)^{1/2}, \end{aligned} \quad (10)$$

where $trace(\cdot)$ is the function summing up the elements on the main diagonal. Figure 7 indicates the involved elements

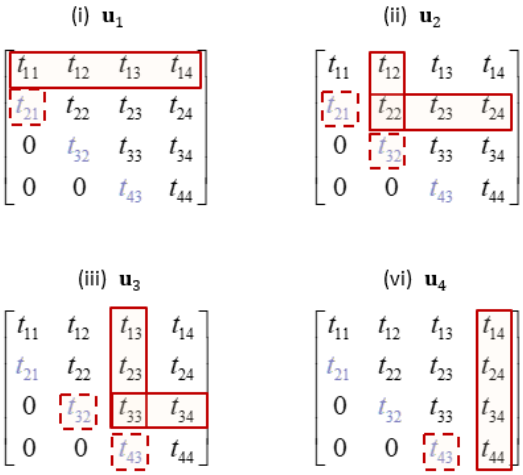

FIGURE 7. Corresponding elements (marked with solid and dashed rectangles) in Schur matrix for each orthonormal vector $\mathbf{u}_k$.

in $\mathbf{T}$ for each individual $\mathbf{u}_k$. Suppose we have $\eta_{k_1} \geq \eta_{k_2} \geq \eta_{k_3} \geq \eta_{k_4}$ with $k_i \in \{1, 2, 3, 4\}$. The predominant vector is the k_1^{th} column vector in $\mathbf{U}$. The watermarking process ought to be taken effect on the 2nd and 3rd elements in that vector as

$$\begin{cases} \hat{u}_{2k_1} = \text{sign}(u_{2k_1}) \times \left(\dfrac{|u_{2k_1}| + |u_{3k_1}|}{2} + (-1)^{w_b+1}\, d \right); \\ \hat{u}_{3k_1} = \text{sign}(u_{3k_1}) \times \left(\dfrac{|u_{2k_1}| + |u_{3k_1}|}{2} + (-1)^{w_b}\, d \right), \end{cases} \quad (11)$$

where the variable d represents the clearance gap in binary watermarking.

D. ORTHONORMAL RECONSTRUCTION

The manipulation within the dominating vector inevitably disturbs the unitary properties of $\mathbf{U}$. That is, the column vectors in $\mathbf{U}$ are no longer orthonormal. An easy way to repair the orthonormality is by means of the Gram Schmidt process [31], [32].

$$\begin{aligned} \mathbf{h}_1 &= \hat{\mathbf{u}}_1, \quad \mathbf{v}_1 = \frac{\mathbf{h}_1}{\|\mathbf{h}_1\|}; \\ \mathbf{h}_2 &= \hat{\mathbf{u}}_2 - \frac{\mathbf{h}_1^T\hat{\mathbf{u}}_2}{\mathbf{h}_1^T\mathbf{h}_1}\hat{\mathbf{u}}_2, \quad \mathbf{v}_2 = \frac{\mathbf{h}_2}{\|\mathbf{h}_2\|}; \\ \mathbf{h}_3 &= \hat{\mathbf{u}}_3 - \frac{\mathbf{h}_1^T\hat{\mathbf{u}}_3}{\mathbf{h}_1^T\mathbf{h}_1}\mathbf{u}_3 - \frac{\mathbf{h}_2^T\hat{\mathbf{u}}_3}{\mathbf{h}_2^T\mathbf{h}_2}\hat{\mathbf{u}}_3, \quad \mathbf{v}_3 = \frac{\mathbf{h}_3}{\|\mathbf{h}_3\|}; \\ \mathbf{h}_4 &= \hat{\mathbf{u}}_4 - \frac{\mathbf{h}_1^T\hat{\mathbf{u}}_4}{\mathbf{h}_1^T\mathbf{h}_1}\hat{\mathbf{u}}_4 - \frac{\mathbf{h}_2^T\hat{\mathbf{u}}_4}{\mathbf{h}_2^T\mathbf{h}_2}\hat{\mathbf{u}}_4 - \frac{\mathbf{h}_3^T\hat{\mathbf{u}}_4}{\mathbf{h}_3^T\mathbf{h}_3}\hat{\mathbf{u}}_4, \quad \mathbf{v}_4 = \frac{\mathbf{h}_4}{\|\mathbf{h}_4\|}, \end{aligned} \quad (12)$$

where $\|\mathbf{h}_i\|$ denotes the Euclidean norm of vector $\mathbf{h}_i$ and $i \in \{1, 2, 3, 4\}$. The use of $\mathbf{V}$ in the matrix recomposition $\mathbf{A}_V = \mathbf{V}\mathbf{T}\mathbf{V}^T$ ensures an exact retrieval of $\mathbf{V}$ and $\mathbf{T}$ from the SD of $\mathbf{A}_V$. Only an accurate restoration of the dominating vector $\mathbf{v}_i$ can guarantee a perfect retrieval of the watermark bit.

E. DISTORTION COMPENSATION

Given that a watermarking bit is now hidden inside the unitary matrix $\mathbf{V}$ through Eqs. (11) and (12), the watermark embedding generates a distortion Γ in terms of the sum squared error between the matrix elements in $\mathbf{A}_V$ and $\mathbf{A}_{\lambda^*}$:

$$\Gamma = \|\mathbf{A}_V - \mathbf{A}_{\lambda^*}\|_{Frob}^2 . \tag{13}$$

Since $\mathbf{A}_V$ is composed of $\mathbf{V}$ and $\mathbf{T}$, it is possible for us to further reduce Γ by modifying $\mathbf{T}$ while keeping $\mathbf{V}$ intact. The content in matrix $\mathbf{T}$ can be divided into several subgroups based on the eigenvalues shown in the diagonal. In case all the eigenvalues are real, the plane formed by $\mathbf{v}_i\mathbf{v}_j^T$ is regarded as an independent vector subspace and t_{ij} can be readjusted individually. The condition is somewhat complicated when SD returns complex eigenvalues, which happen when $t_{kk} = t_{ll}$ and $t_{kl} \neq 0$ with $l = k+1$. Accordingly, $\mathbf{v}_k$ and $\mathbf{v}_l$ form a joint subspace that is not separable. We therefore assign both the indexes k and l to the m^{th} subgroup, termed G_m. When dealing with the vectors in subgroup G_m, any entanglement with $\mathbf{v}_k$ shall always involve $\mathbf{v}_l$. The plane $\mathbf{P}^{(mn)}$ spanned by the m^{th} and n^{th} subgroups thus becomes

$$\mathbf{P}^{(mn)} = \sum_{i\in G_m}\sum_{j\in G_n} [\![t_{ij} \neq 0]\!]\, t_{ij}\mathbf{v}_i\mathbf{v}_j^T , \tag{14}$$

where $[\![t_{ij} \neq 0]\!]$ represents a logical operation, which returns 1 if $t_{ij} \neq 0$ is true and 0 otherwise. Summing all $\mathbf{P}^{(mn)}$ restores $\mathbf{A}_V$, i.e.,

$$\mathbf{A}_V = \sum_{m=1}^{K_{sub}}\sum_{n=1}^{K_{sub}} \mathbf{P}^{(mn)}, \tag{15}$$

where K_{sub} denotes the number of subgroups.

In accordance with Eq. (14), the adjustment of t_{ij}'s in $\mathbf{P}^{(mn)}$ is equivalent to reassigning a multiplicative factor ξ_{mn} to $\mathbf{P}^{(mn)}$. Hence the optimal $\hat{\xi}_{mn}$ that achieves the minimum distortion can be derived from

$$\hat{\xi}_{mn} = \min_{\xi_{mn}} \left\| \mathbf{A}_{\lambda^*} - \sum_{m=1}^{K_{sub}}\sum_{n=1}^{K_{sub}} \xi_{mn}\mathbf{P}^{(mn)} \right\|_{Frob}^2 . \tag{16}$$

It can be shown that

$$\hat{\xi}_{mn} = \frac{\sum_{i=1}^{4}\sum_{j=1}^{4} a_{ij}^{(\lambda^*)} p_{ij}^{(mn)}}{\sum_{i=1}^{4}\sum_{j=1}^{4} p_{ij}^{(mn)} p_{ij}^{(mn)}}, \tag{17}$$

where $a_{ij}^{(\lambda^*)}$ denotes the $(i,j)^{th}$ element of $\mathbf{A}_{\lambda^*}$. The involved t_{ij}'s are then modified as

$$\hat{t}_{ij} = \hat{\xi}_{ij} t_{ij}, \quad \forall\, i \in G_m; \quad j \in G_n. \tag{18}$$

Once all $\hat{t}_{ij}$'s are available, we recompose the watermarked matrix using

$$\hat{\mathbf{A}}_V = \mathbf{V}\hat{\mathbf{T}}V^T . \tag{19}$$

F. RECURSIVE REGULATION

To restore the average level, we need to rescale the level of $\hat{\mathbf{A}}_V$ to match up with $\mathbf{A}_{\lambda^*}$ and then shift it back to the original level, previously denoted as $\bar{A}$. A possible result is of the following form:

$$\begin{aligned}\hat{\mathbf{A}}^{(opt.1)} &= \hat{\mathbf{A}}_V \frac{\lambda}{\overline{\hat{A}_V}} + \left(\bar{A} - \lambda\right)\mathbf{1}_{4\times 4} \\ &= \mathbf{V}\left(\frac{\lambda}{\overline{\hat{A}_V}}\hat{\mathbf{T}}\right)\mathbf{V}^T + \left(\bar{A} - \lambda\right)\mathbf{1}_{4\times 4},\end{aligned} \tag{20}$$

where $\overline{\hat{A}_V}$ denotes the average pixel value contained in $\hat{\mathbf{A}}_V$. Theoretically, $\hat{\mathbf{A}}^{(opt.1)}$ holds an average level identical to the original $\bar{A}$. The application of SD to $\hat{\mathbf{A}}^{(opt.1)} + \left(\lambda - \bar{\hat{A}}^{(opt.1)}\right)\mathbf{1}_{4\times 4}$ brings the same unitary matrix $\mathbf{V}$ that leads to a correction extraction of the watermark bit.

The last step to complete the watermark embedding is to cast $\hat{\mathbf{A}}^{(opt.1)}$ into an unsigned 8-bit integer type, i.e. $\hat{\mathbf{A}}_{\text{uint8}}^{(opt.1)} = f_{\text{uint8}}\left(\hat{\mathbf{A}}^{(opt.1)}\right)$, where $f_{\text{uint8}}(\cdot)$ takes effect on every element of the input matrix. Note that in Eq. (20), the operation of scaling $\hat{\mathbf{T}}$ by $\lambda/\overline{\hat{A}_V}$ contradicts the primal intention of reducing the distortion. A compromise can be reached by examining a tentative substitute $\hat{\mathbf{A}}^{(opt.2)}$, wherein the scaling is deliberately omitted.

$$\hat{\mathbf{A}}^{(opt.2)} = \hat{\mathbf{A}}_V + \left(\bar{A} - \lambda\right)\mathbf{1}_{4\times 4}. \tag{21}$$

The unsigned 8-bit integer version of $\hat{\mathbf{A}}^{(opt.2)}$ is acquired as $\hat{\mathbf{A}}_{\text{uint8}}^{(opt.2)} = f_{\text{uint8}}\left(\hat{\mathbf{A}}^{(opt.2)}\right)$. If the watermark bit extracted from $\hat{\mathbf{A}}_{\text{uint8}}^{(opt.2)}$ consists with the previously embedded w_b, $\hat{\mathbf{A}}_{\text{uint8}}^{(opt.2)}$ serves as the final output directly. In case of a wrong outcome, we then try $\hat{\mathbf{A}}_{\text{uint8}}^{(opt.1)}$. The employment of $\hat{\mathbf{A}}_{\text{uint8}}^{(opt.1)}$ usually renders a correct extraction of the watermark bit, due to the fact that $\hat{\mathbf{A}}^{(opt.1)}$ is the ideal watermarked matrix. Nonetheless, in rare situations a false outcome may still appear, as some elements of $\hat{\mathbf{A}}^{(opt.1)}$ fall far away from the allowable range, i.e., (0,255). A consequential regulation is therefore necessary. Here we resort a recursive approach, which adopts $\hat{\mathbf{A}}_{\text{uint8}}^{(opt.1)}$ as the input and rerun the foregoing processes. The recursive iteration may however fall into an endless loop as long as a fixed $\mathbf{A}_{\lambda^*}$ is used in the distortion compensation (as shown in Eqs. (16)-(19)). To break the endless loop, we modify $\mathbf{A}_{\lambda^*}$ as below for each subsequent iteration.

$$\mathbf{A}_{\lambda^*}^{(n+1)} = \mathbf{A}_{\lambda^*}^{(n)} + (-1)^{w_b+1}\begin{bmatrix} 0 & 0 & 0 & 0 \\ 0.5 & 0.5 & 0.5 & 0.5 \\ -0.5 & -0.5 & -0.5 & -0.5 \\ 0 & 0 & 0 & 0 \end{bmatrix}, \tag{22}$$

where the superscript n within the parentheses denotes the iteration number. In Eq. (22), adding 0.5 to the second row along with subtracting 0.5 from the third row of the matrix establishes a favor condition for $w_b = 1$. On the contrary, subtracting values from the second row and adding values to

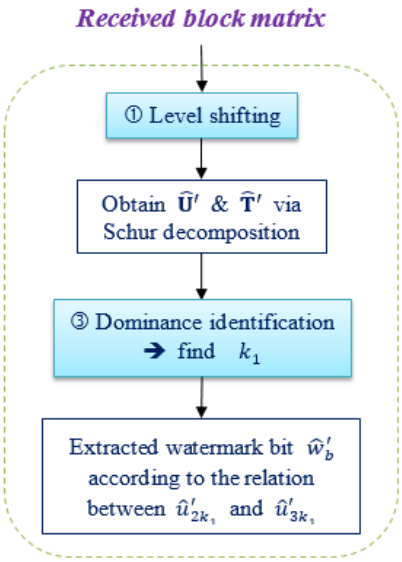

FIGURE 8. Extraction procedure of the reinforced SD-based watermarking scheme.

the third row has a preference for $w_b = 0$. The use of Eq. (22) in the recursive iteration can resolves the ultimate difficulty. Eventually, the procedure shown in Fig. 5 assures an accurate watermark retrieval.

G. WATERMARK EXTRACTION

In comparison with the complication of watermark embedding, the process of watermark extraction is rather straightforward. As shown in Fig. 8, only level shifting and dominance identification are required in the watermark extraction procedure. Figure 8 also represents the process required in the second and third decision boxes shown in Fig. 5. The watermark bit hidden in each image block can be obtained in accordance with Eq. (3).

IV. PERFORMANCE EVALUATION

The testing materials comprised twelve different 24-bit color images (512 × 512 pixels) selected from the CVG-UGR image database [33]. Figure 9 shows these twelve host images, which consisted of "*Lena*", "*Baboon*", "*Avion*", "*Peppers*", "*Blueeye*", "*Bluheron*", "*Elephant*", "*Fiore*", "*Frog*", "*Goldgate*", "*London*" and "*Manhatan*". We compared the performance of the proposed RSD with four other SD-based schemes, namely, the PSD [26], LSD [29], ISD [24] and ASD [30] previously discussed in the introduction section. To verify the effect due to distortion compensation, the comparison also took account of the RSD without distortion compensation (herein referred to as RSDwo). All the compared methods belong to the category of blind watermarking in the sense that the extraction of the watermark does not require the presence of the original host image. Furthermore, in order to provide a baseline for comparison, we also implemented a non-blind watermarking scheme based on the SD framework. For this non-blind scheme (herein referred to as NSD), the magnitude of the second element (i.e., $|u_{2k_1}|$) in the k_1^{th} dominant vector is chosen as the reference object. To embed a binary bit w_b into the designated image block, the NSD alters u_{2k} as

$$\hat{u}_{2k_1} = \text{sign}\left(u_{2k_1}\right) \max\left\{0,\ |u_{2k_1}| + (-1)^{w_b+1} d_{nb}\right\}, \tag{23}$$

where d_{nb} denotes the clearance gap used in the NSD. Following the adjustment of $\hat{u}_{2k_1}$, all the other matrix elements involved in the Schur decomposition are modified using the techniques discussed in Section III. During watermark extraction, the watermark bit can be recovered by examining whether the acquired $|\hat{u}'_{2k_1}|$ is greater than $|u_{2k_1}|$, of which the value is readily available because of the non-blind assumption.

$$\hat{w}_b' = \begin{cases} 1, & \text{if } |\hat{u}'_{2k_1}| \geq |u_{2k_1}|; \\ 0, & \text{otherwise.} \end{cases} \tag{24}$$

In this study, we adopted the RGB model to represent a color image, wherein each pixel requires three discrete values to characterize the color intensity in red, green, and blue. Watermarking embedding and extraction in color images were actually performed on the red, green, and blue channels individually. To reconstruct a color watermark, we gathered all binary bits retrieved from these three channels in proper order.

According to the specifications in the literature [24], [26], [29], [30], the PSD, LSD, ISD, and ASD schemes were designed to embed a 24-bit color image logo of size 32 × 32 into 4 × 4 non-overlapped matrix blocks drawn from a 24-bit color image of size 512 × 512. This implies that only half of the image blocks were involved in the embedding process. However, the authors in [24], [26], [29], [30] did not specifically point out how to select among the available image blocks. For a fair comparison, we conducted a full binary embedding using a 24-bit color image logo of size 64 × 32. That is, every 4 × 4 block of the host image must contain one bit after the watermarking process. Figure 10 presents the watermark logo. The size of the watermark logo was converted from 64 × 32 × 24 to 128 × 128 × 3 for one-to-one correspondence. To enhance the security, the resultant watermark logo was scrambled using Arnold transform [34] with chaotic mapping [35]. The final outcome of the scrambled watermark contained 24638 "1's" and 24514 "0's" in total.

The metrics used to measure the amount of distortion introduced by watermarking included the peak signal-to-noise ratio (PSNR), weighted peak signal-to-noise ratio (WPSNR), and mean structural similarity (MSSIM). PSNR refers to the numerical difference between the original and watermarked images. MSSIM is a statistical method that compares blocks of a given host image with their counterparts of the watermarked image. The MSSIM metric has been shown to give results closely matching subjective evaluation [36]. The definitions of PSNR, WPSNR, and MSSIM are given

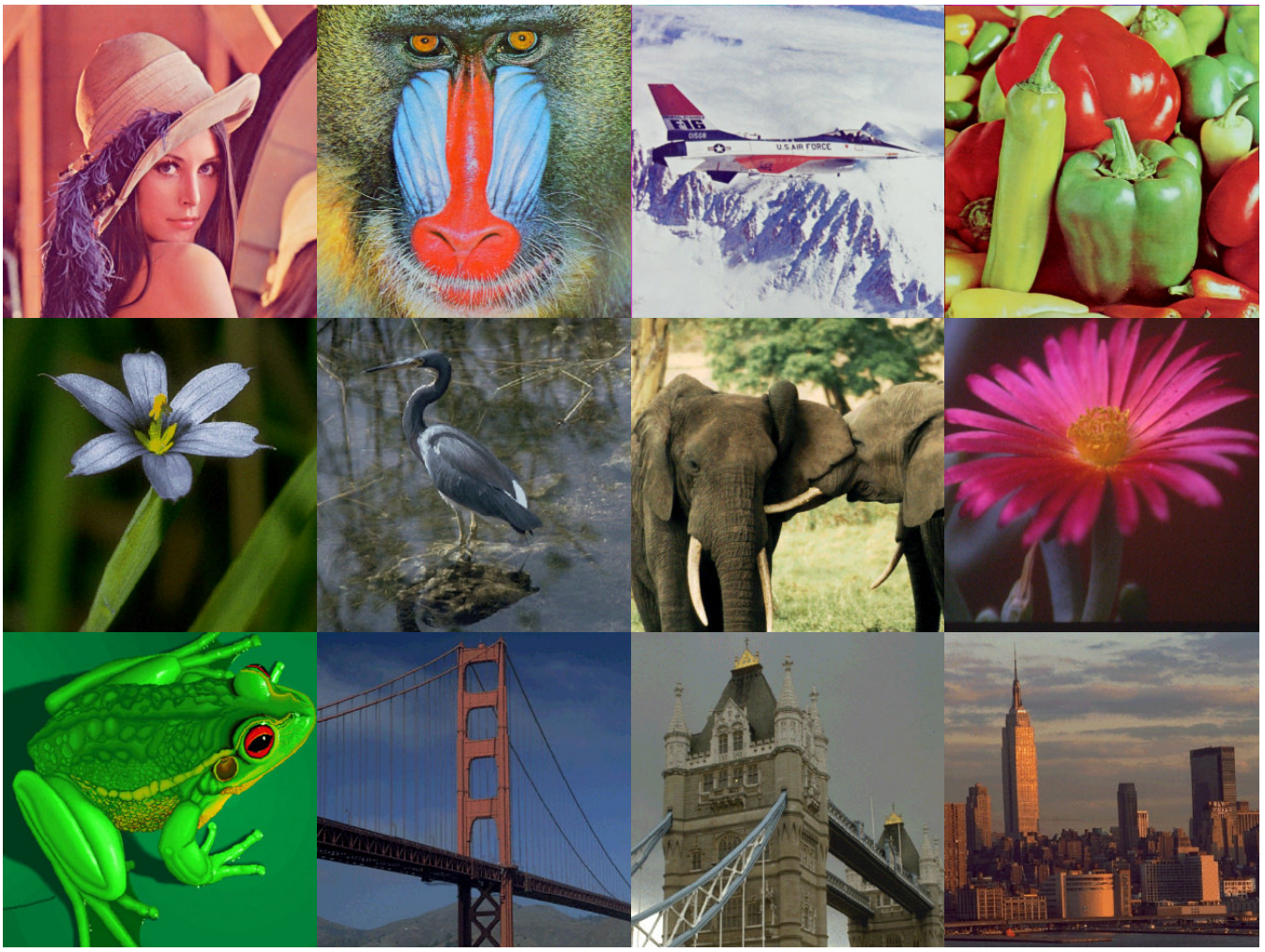

FIGURE 9. The testing materials.

below:

$$\mathrm{PSNR}(\mathbf{I}, \hat{\mathbf{I}}) = \frac{1}{C}\sum_{c=1}^{C} 10 \times \log_{10}\left(\frac{255^2}{\frac{1}{X\times Y}\sum_{x=1}^{X}\sum_{y=1}^{Y}(I_{c,x,y} - \hat{I}_{c,x,y})^2}\right); \tag{25}$$

$$\mathrm{WPSNR}(\mathbf{I}, \hat{\mathbf{I}}) = \frac{1}{C}\sum_{c=1}^{C} 10 \times \log_{10}\left(\frac{L_{\max}^2}{\frac{\mathrm{NVF}^2}{X\times Y}\sum_{x=1}^{X}\sum_{y=1}^{Y}(I_{c,x,y} - \hat{I}_{c,x,y})^2}\right); \tag{26}$$

$$\mathrm{MSSIM}(\mathbf{I}, \hat{\mathbf{I}}) = \frac{1}{C \times R \times S} \times \sum_{c=1}^{C}\sum_{r=1}^{R}\sum_{s=1}^{S} \mathrm{SSIM}(B_{c,r,s}, \hat{B}_{c,r,s}), \tag{27}$$

where the expression $X \times Y$ indicates the size of the host color image. Symbol C (= 3) denotes the number of channels for a RGB color image. $\mathbf{I} = \{I_{c,x,y}\}$ and $\hat{\mathbf{I}} = \{\hat{I}_{c,x,y}\}$ respectively represent the host and watermarked images. $L_{\max}$ is the maximum value of luminance level. NVF denotes the noise visibility function for texture masking. $SSIM(\cdot)$ is the function used to compute the degree of similarity between the original image block $B_{c,r,s}$ and watermarked image block $\hat{B}_{c,r,s}$ at the (r, s)$^{\text{th}}$ local window of the c$^{\text{th}}$ channel [36].

While in the presence of commonly encountered attacks, the performance of watermarking detection were assessed based on the bit error rate (BER) and normalized cross-correlation (NCC) [37], which are respectively defined as

$$\mathrm{BER}(\mathbf{W}, \tilde{\mathbf{W}}) = \frac{1}{C \times P \times Q}\sum_{c=1}^{3}\sum_{p=1}^{P}\sum_{q=1}^{Q}\left|w_{c,p,q} - \tilde{w}_{c,p,q}\right|; \tag{28}$$

$$\mathrm{NCC}(\mathbf{W}, \tilde{\mathbf{W}}) = \frac{\sum_{c=1}^{3}\sum_{p=1}^{P}\sum_{q=1}^{Q} w_{c,p,q} \times \tilde{w}_{c,p,q}}{\sqrt{\sum_{c=1}^{3}\sum_{p=1}^{P}\sum_{q=1}^{Q} w_{c,p,q}^2 \times \sum_{c=1}^{3}\sum_{p=1}^{P}\sum_{q=1}^{Q} \tilde{w}_{c,p,q}^2}}, \tag{29}$$

where $P \times Q$ signifies the size of the watermark image. Symbols $\mathbf{W} = \{w_{c,p,q}\}$ and $\tilde{\mathbf{W}} = \{\tilde{w}_{c,p,q}\}$ denote the original and extracted watermark images, respectively. The tilde atop the variable indicates that the watermark may suffer possible attacks.

For a fair comparison, we cautiously adjusted the controlling parameters for the investigated schemes so that the resulting PSNR values were close to each other. Specifically, the average PSNR value obtained from the RSDwo was close to that from PSD [26], and the average PSNR obtained from the NSD and RSD were close to those from LSD [29]. For the proposed RSDwo and RSD the level shifting parameter λ was 64 and the clearance gap d was set as 0.015. In the implementation of PSD [26], the gap T was chosen as 0.0016. As for the LSD [29], the embedding strength K and embedding factor Δ were assigned as 30 and 0.78, respectively. While implementing ISD [24], the threshold value T and embedding factor β were 0.005 and 0.2, respectively. The quantization step T was 40 in the implementation of ASD [30]. Finally, the clearance gap d_{nb} was set as 0.048 for NSD to render a PSNR approximate to that obtained from RSD.

A. TIME COMPLEXITY

Our first concern is the computational requirement of the proposed RSD scheme. When analyzing time complexity, we adopted the big O notation to characterize the asymptomatic behaviors of relevant operations considered in the proposed SD-based watermarking scheme. The mainly time complexity of the six basic processing modules (namely, ''Schur decomposition'', ''dominance identification'', ''orthonormal reconstruction'', ''distortion compensation'', ''matrix recomposition'', and ''recursive regulation'') participating in the proposed RSD are $O(\frac{8}{3}n^3)$, $O(n^2)$, $O(2n^3)$, $O(3n^2)$, $O(2n^3)$ and $O(\frac{8}{3}n^3)$ respectively with the single image block size $n \times n$. Hence the overall time complexity for a color image of $\mathrm{N} \times \mathrm{N}$ pixels is approximately three times the summation, i.e., $3 \times \frac{N \times N}{n \times n} O(\frac{28}{3}n^3 + 4n^2)$.

B. IMPERCEPTIBILITY TEST

The performance in imperceptibility can be evaluated by inspecting the effect due to the embedding of the watermark logo (as in Fig. 10) into the host image (as in Fig. 9). Note that the PSNR also reflects the embedding strength imposed by a watermarking scheme. Figure 11 shows part of watermarked images (namely, ''*Lena*'', ''*Baboon*'', ''*Avion*'' and ''*Peppers*'') obtained from the compared schemes. As illustrated in Fig. 11, all the watermarked images seldom display traceable flaws caused by the watermarking process. Nonetheless, a careful examination reveals that a slight sawtooth

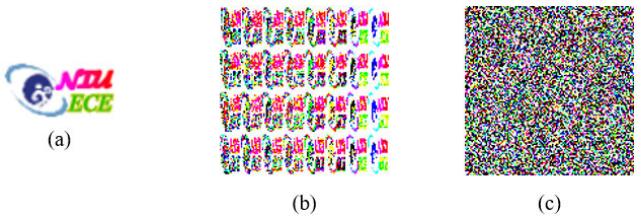

FIGURE 10. Illustration of the watermark image: (a) 24-bit color watermark image of size 64 × 32 × 24, (b) reshaped watermark of size 128 × 128 × 3, and (c) its scrambled version (128 × 128 × 3).

phenomenon may occur at some edges in ''*Lena*'' and ''*Avion*'' images after the process of PSD, ISD, RSDwo, RSD, and NSD. The sawtooth phenomenon is most noticeable in PSD, followed by ISD. The quality degradation due to the proposed RSD scheme is just minor. Such a phenomenon can be attributed to the fact that these four schemes (namely, PSD, ISD, RSD, and NSD) are designed to modify principal elements in the unitary matrix $\mathbf{U}$. The heavier the modification is, the greater the difference emerges between the original and watermarked image blocks. By contrast, LSD and ASD embed the watermark bit by modifying the largest eigenvalue of the Schur matrix, thus primarily affecting the pixel intensity. The textual structure within each image block can still be preserved to a large extent. Nonetheless, LSD and ASD may suffer the block effect if abrupt discontinuities occur along neighboring image blocks.

Table 1 lists the statistics derived from measured PSNRs, WPSNRs, and MSSIMs for all compared schemes. It can be seen that the WPSNRs and PSNRs of the compared schemes share a general trend. That is, a scheme with a higher PSNR is usually associated with a higher WPSNR. However, the WPSNR values of LSD and ASD were comparatively small. The reason can be attributed to the fact that these two schemes modify the pixel values over the entire image block while performing watermark embedding. Although the watermarked images processed by PSD had the lowest average PSNR value, its MSSIM value was not the lowest. LSD had a relatively high average PSNR, but its average MSSIM was rather low. ASD held the lowest MSSIM value of 0.944, while its PSNR was controlled at 36.36 dB. As for the RSDwo (i.e., the RSD without distortion compensation), the resulting PSNR value was close to PSD. Once the compensation was activated, the average PSNR value was increased by approximately 2.47 dB; meanwhile the MSSIM value was also improved.

C. ROBUSTNESS TEST

The robustness of all the SD-based schemes under common attacks was examined using the BER and NCC defined in Eqs. (27) and (28), respectively. The attack types consisted of image compression, cropping, noise corruption, filtering and luminance adjustment, which are specified below:

A1. Image compression / JPEG: The JPEG standard with the quality factor (QF) chosen from $\{70, 80, 90\}$ is applied to the test image.

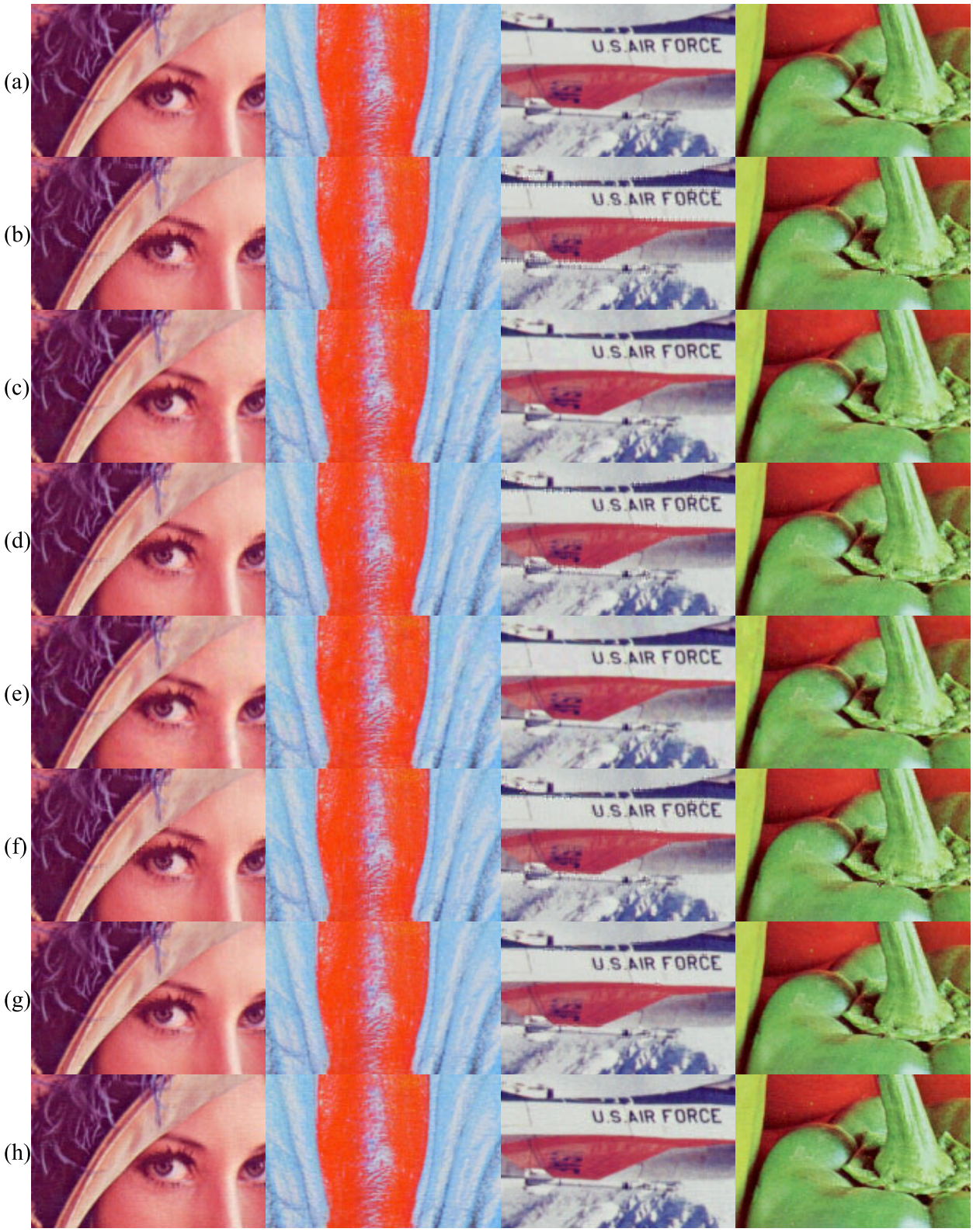

FIGURE 11. Close-ups of (a) original image and the results obtained by (b) PSD, (c) LSD, (d) ISD, (e) ASD, (f) RSDwo, (g) RSD, and (h)NSD. Images from left to right are "*Lena*", "*Baboon*", "*Avion*" and "*Peppers*".

TABLE 1. Mean and standard deviation of PSNR (in dB), WPSNR (in dB), and MSSIM for the compared methods.

	PSNR							WPSNR							MSSIM					
	PSD	LSD	ISD	ASD	The proposed RSDwo	The proposed RSD	NSD	PSD	LSD	ISD	ASD	The proposed RSDwo	The proposed RSD	NSD	PSD	LSD	ISD	ASD	The proposed RSDwo	The proposed RSD
Lena	38.44	38.53	40.15	36.55	37.73	40.05	38.64	56.58	45.21	56.85	43.17	55.54	57.77	55.67	0.997	0.997	0.998	0.995	0.996	0.997
Baboon	27.61	38.54	30.22	36.49	29.29	31.75	38.51	45.63	45.40	48.11	43.16	46.93	48.96	54.85	0.951	0.995	0.973	0.992	0.966	0.979
Avion	35.06	38.49	37.02	36.43	35.59	38.00	38.61	53.06	45.13	53.83	43.01	53.17	55.32	55.58	0.966	0.843	0.935	0.805	0.886	0.923
Peppers	36.06	38.45	38.26	36.40	35.94	38.88	38.76	54.09	45.38	55.52	43.02	52.69	56.14	55.45	0.995	0.996	0.997	0.993	0.994	0.997
Blueeye	37.41	38.23	39.77	35.73	37.44	39.82	39.34	55.48	46.33	57.46	42.32	54.62	56.88	55.10	0.988	0.959	0.992	0.918	0.975	0.985
Bluheron	36.56	38.50	38.85	36.44	36.57	39.03	38.88	54.53	45.23	56.17	43.10	54.39	56.45	55.94	0.961	0.956	0.974	0.932	0.945	0.967
Elephant	36.43	38.56	38.48	36.43	36.20	38.66	38.77	54.57	45.43	55.83	43.08	53.46	56.09	55.63	0.983	0.974	0.989	0.958	0.971	0.982
Fiore	37.25	38.56	39.52	36.55	36.95	39.14	38.65	56.94	45.31	58.40	43.18	55.32	57.09	55.48	0.985	0.991	0.991	0.985	0.984	0.990
Frog	35.98	38.03	38.71	35.68	36.25	39.04	39.13	54.86	46.01	57.28	42.25	53.27	56.38	54.98	0.997	0.996	0.999	0.993	0.996	0.998
Goldgate	38.52	38.57	40.80	36.47	37.85	40.23	38.82	56.43	45.28	57.70	43.01	55.15	57.68	55.68	0.987	0.985	0.992	0.976	0.982	0.989
London	37.09	39.06	39.54	36.54	37.02	39.50	38.79	54.98	45.77	56.40	43.11	54.37	57.01	55.72	0.968	0.893	0.958	0.844	0.888	0.922
Manhatan	35.70	38.49	37.90	36.67	35.92	38.27	38.80	53.90	45.20	55.42	43.26	53.71	55.43	55.68	0.970	0.950	0.976	0.933	0.946	0.966
Overall mean	**36.01**	**38.50**	**38.27**	**36.36**	**36.06**	**38.53**	**38.81**	**54.25**	**45.47**	**55.75**	**42.97**	**53.55**	**55.93**	**55.48**	**0.979**	**0.963**	**0.981**	**0.944**	**0.961**	**0.975**
Standard deviation	2.84	0.24	2.62	0.32	2.26	2.15	0.23	2.95	0.37	2.70	0.33	2.28	2.33	0.33	0.015	0.048	0.019	0.062	0.038	0.027

A2. Image compression / JPEG2000: The JPEG2000 standard with the compression ratio (CR) chosen from {1, 3, 6, 9} is applied to the test image.
A3. Cropping (I): 25% of the test image on the left side is cropped.
A4. Cropping (II): 25% of the test image on the left upper corner is cropped.
A5. Filtering (I): a Gaussian lowpass filter is applied to the test image.
A6. Filtering (II): an unsharp masking filter is applied to the test image.
A7. Luminance adjustment / brightening: each pixel value of the test image is increased by 20.
A8. Luminance adjustment / darkening: each pixel value of the test image is decreased by 20.
A9. Noise corruption: the test image is corrupted by the salt & pepper noise with 1% intensity.
A10. Contrast enhancement: a histogram equalizer is applied to the test image.

Figure 12 presents the image logos acquired from the watermarked ''Manhatan'' images for the compared SD-based schemes. Here we chose ''Manhatan'' as the representative because the BERs derived from this image approximated the average values obtained from the test images. As seen in Fig. 12, the proposed RSD and NSD schemes perfectly extract the watermark when the attack is absent; however, different degrees of errors occur for the other four schemes. Such results indicate that the proposed scheme can be deployed in a normal situation, which requires the embedded information to be retrieved and transmitted without any error. According to the results in Figure 12, all SD-based schemes seem to lack sufficient resistance against JPEG attacks. In JPEG compression with a quality factor lower than 60, the binary information contained in watermarked image appears seriously perturbed and the watermark is determined mostly by guessing. The reason can be ascribed to the fact that they all rely on the local inequality across adjacent row pixels to hide the watermark. Throughout the JPEG compression, the minor variation in row pixels is substantially smoothed away. It is the smoothing effect that ruins the embedded watermark.

The watermark acquired via PSD is barely recognizable even in the absence of attacks. By contrast, ISD renders a rather clear watermark when no attack is present. The visual inspections with respect to the recovered image logos confirm that ISD is generally superior to PSD in terms of robustness. Overall, the performance of LSD is moderate. LSD can survive in the attacks like low-ratio JPEG2000 compression (A2/CR 1, A2/CR 3 and A2/CR 6), Gaussian lowpass filter (A5), and noise corruption (A9). However, it completely fails in the attacks of unsharp filtering (A6) and contrast enhancement (A10). In the particular cases of luminance adjustment (i.e., A7 and A8), the variation of the intensity level directly affects the largest eigenvalue, wherein the watermark is inserted. The recovered image logo unexpectedly looks inverted. The image inversion is merely the consequence of classifying most watermark bits into their antipodal values. Finally, regardless of the participation of distortion compensation, the image logos extracted by RSD are most recognizable, despite that parts of the image logos appear somewhat blurred in the cases of high JPEG2000 image compression (A2/CR 9) and cropping (A3 and A4). ASD shows better robustness than RSD in the image compression attacks (A1 and A2), but it completely lacks the ability to withstand the attacks of unsharp filtering (A6) and contrast enhancement (A10).

Table 2 lists the average BER values of the twelve images for the compared schemes. Based on our experience, an image logo with a BER less than 12.5% can be assumed as visually recognizable. Just like the condition discussed in the previous paragraph, the image logo retrieved via the PSD scheme could not be recognized even under the absence of any attacks. ISD showed certain improvement over PSD. Especially, in attacks such as JPEG2000 compression (A2/CR 1),

FIGURE 12. Watermark images extracted from the watermarked " *Manhatan* " images in the presence of various attack.

luminance adjustment (A7 and A8), noise corruption (A9) and contrast enhancement (A10), the BERs obtained by ISD were below 12.5%. Compared with PSD and ISD, the proposed RSD evidently showed enhancement in robustness no matter what image attack was. For LSD, ASD and RSD, the mild BERs (near 12.5%) in the attacks A3 and A4 should be considered reasonably acceptable, owing to the fact that it is simply the result of pure guess in a loss of 25% image.

Except unsharp filtering (A6), luminance adjustment (A7 and A8) and contrast enhancement (A10), LSD generally provided better resistance than ISD. The proposed RSD scheme was able to outperform LSD in attacks such as low JPEG2000 image compression (A2/CR 1 and A2/CR

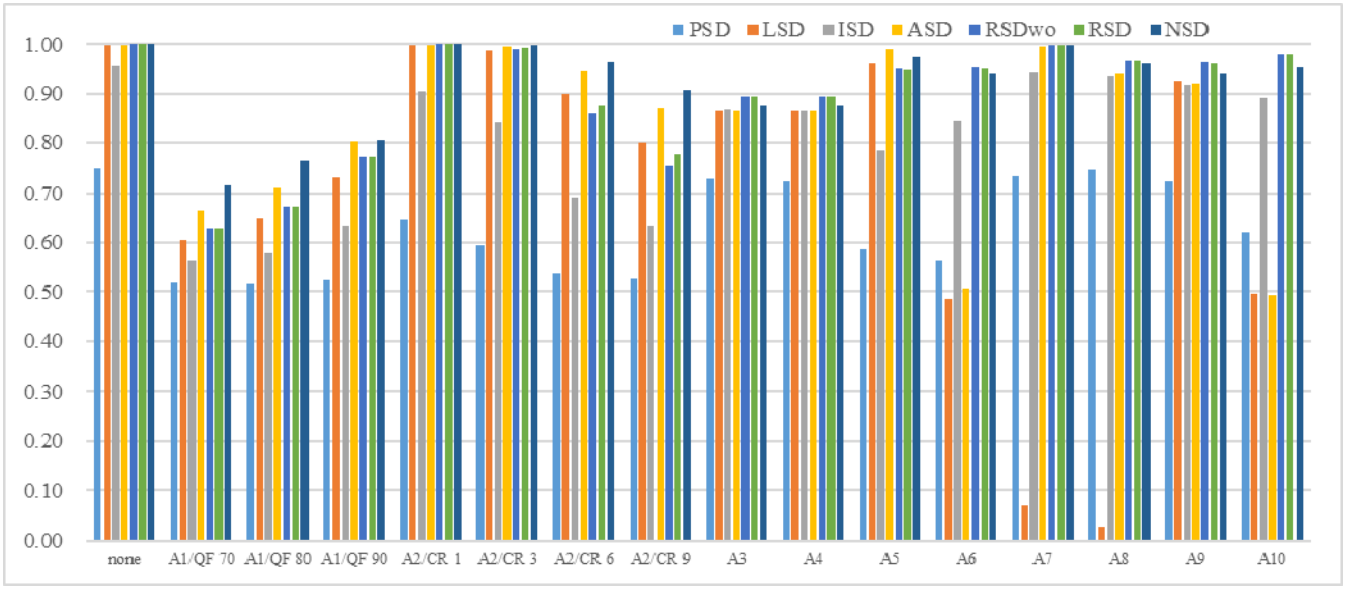

FIGURE 13. Average NCCs for the compared methods in the presence of various attacks.

TABLE 2. Average BERs (in percentage) for the compared methods in the presence of various attacks.

	PSD	LSD	ISD	ASD	The proposed			NSD
					RSDwo	RSD	p-value	
none	26.52	0.14	4.80	0.06	0.00	0.00	-	0.00
A1/QF 70	49.42	39.09	44.90	33.83	38.66	38.76	0.872	27.43
A1/QF 80	49.16	34.77	42.81	28.99	33.30	33.47	0.751	23.13
A1/QF 90	48.12	26.57	36.97	19.80	22.81	22.96	0.720	19.09
A2/CR 1	35.79	0.28	9.81	0.11	0.01	0.01	0.989	0.00
A2/CR 3	41.11	1.32	16.02	0.39	0.93	0.75	0.777	0.10
A2/CR 6	46.79	10.10	31.31	5.54	14.32	12.63	0.591	3.19
A2/CR 9	47.95	19.77	37.24	13.19	25.07	22.79	0.468	8.13
A3	31.93	12.65	15.92	12.60	12.44	12.44	-	12.53
A4	32.53	12.66	16.24	12.59	12.46	12.46	-	12.53
A5	42.30	3.76	22.02	1.05	4.99	5.09	0.933	2.25
A6	44.02	50.78	15.85	48.10	4.53	4.93	0.832	5.45
A7	27.42	95.36	5.43	0.53	0.29	0.28	0.976	0.26
A8	27.70	91.26	7.33	5.47	3.82	3.99	0.946	3.76
A9	28.95	7.61	8.51	7.90	3.70	3.72	0.805	5.61
A10	40.71	50.33	10.67	50.99	2.14	2.12	0.968	4.19

3), unsharp filtering (A6), luminance adjustment (A7 and A8), noise corruption (A9) and contrast enhancement (A10); however, its performance slightly degraded when dealing with Gaussian lowpass filtering (A5) and JPEG2000 image compression using a ratio greater than 3.

For the data under the column named "the proposed" in Table 2, the resultant BERs of the RSD and RSDwo were slightly different. The compensation improved the ability to combat JPEG2000 compression (A2), luminance adjustment for brightening (A7) and contrast enhancement (A10); however, the compensation seemed to weaken the resistance to attacks such as JPEG compression (A1/QF 70 and A1/QF 90), filtering (A5 and A6), luminance adjustment for darkening (A8) and noise corruption (A9). To verify whether the compensation affects the BER, we conducted a one-way ANOVA based on the BERs obtained from the twelves test images. Table 2 also contains the resultant p-values drawn from the test data. In the cases of "none", "A3", and "A4", the associated p-values were marked as dashes because the proposed RSD resulted in a constant BER regardless of the presence of compensation. As the resultant p-value were distributed from 0.468 to 0.989, the change in the BER means caused by the compensation was statistically insignificant. In combination of the results in Table 1, it is concluded that the employment of distortion compensation method is conducive to the imperceptibility of the watermark but harmless to the robustness.

As listed in the last column of Table 2, the non-blind scheme (i.e., NSD) exhibited noticeable improvement in resisting JPEG and JPEG2000 compression attacks. However, it did not show any obvious advantage against unsharp filtering (A6), noise corruption (A9) and contrast enhancement (A10). Overall, the use of NSD may contribute to the performance in robustness for certain types of attacks; however, it requires a priori information before carrying out watermark extraction.

The NCC metric specified in Eq. (28) presents another aspect of the robustness against various attacks. Figure 13 shows the histograms of the average NCC values for the compared watermarking schemes. As revealed in this figure, the NCCs exhibited a similar tendency analogous to the BERs. Among the five blind SD-based schemes, ASD generally showed the best performance in the presence of the image compression attacks (A1 and A2), but it could not survive attacks A6 and A10. By contrast, except for the JPEG compression with low quality factors, RSD demonstrated sufficient robustness against the commonly encountered attacks.

D. EFFECT OF DIFFERENT COLOR MODELS

Our last concern was focused on the color issue. In fact, a color image can be thought of as a composite of three layers

TABLE 3. Average BERs (in percentage) for the proposed RSD in HSV, YCbCr, and RGB color domains.

	HSV (PSNR: 31.84)				YCbCr (PSNR: 36.01)				RGB (PSNR: 38.53)			
	H	S	V	mean	Y	Cb	Cr	mean	R	G	B	mean
none	5.68	1.45	0.00	2.38	0.03	0.06	0.03	0.04	0.00	0.00	0.00	0.00
A1/QF 70	49.21	51.16	37.78	46.05	31.41	49.46	52.48	44.45	39.39	35.99	40.89	38.76
A1/QF 80	48.43	51.70	32.94	44.36	22.37	49.05	52.70	41.37	34.34	29.25	36.81	33.47
A1/QF 90	46.42	51.80	24.32	40.85	7.13	47.06	50.06	34.75	24.58	15.74	28.55	22.96
A2/CR 1	12.01	4.69	0.01	5.57	0.03	0.09	0.04	0.05	0.01	0.01	0.02	0.01
A2/CR 3	16.90	14.43	2.22	11.18	0.13	0.20	0.57	0.30	1.08	0.29	0.87	0.75
A2/CR 6	32.83	38.65	15.69	29.06	5.99	5.59	13.97	8.52	14.85	8.39	14.65	12.63
A2/CR 9	40.92	45.07	25.96	37.32	13.40	21.27	34.63	23.10	24.81	18.31	25.26	22.79
A3	16.60	13.51	12.60	14.24	12.37	12.44	12.62	12.48	12.35	12.38	12.60	12.44
A4	16.38	13.89	12.51	14.26	12.25	12.71	12.54	12.50	12.22	12.65	12.51	12.46
A5	12.38	11.61	6.52	10.17	5.13	0.58	0.63	2.11	5.16	5.51	4.61	5.09
A6	37.71	25.34	7.57	23.54	3.83	0.69	0.57	1.69	4.92	4.45	5.42	4.93
A7	5.70	2.96	0.77	3.14	0.12	0.18	0.81	0.37	0.59	0.17	0.09	0.28
A8	8.02	12.73	0.78	7.18	2.04	6.56	4.60	4.40	4.23	1.58	6.16	3.99
A9	12.83	10.42	6.28	9.84	7.79	8.69	7.47	7.99	3.65	3.82	3.69	3.72
A10	44.51	36.16	16.17	32.28	1.90	3.76	2.61	2.76	2.06	2.12	2.18	2.12

of images with pure red, green, and blue. In the embedding phase, we applied the watermarking scheme to the red, green, and blue layers separately. Since each color layer allows 256 different intensity levels, the processing with respect to each layer is equivalent to that required for an 8-bit gray-scale image. Consequently, the computational complexity of the proposed color image watermarking scheme is approximately 3 times that demanded by a gray image of the same size. Likewise, the payload capacity for a color image is triple the amount for the gray image of the same size.

In order to verify what benefit can color image watermarking have on accuracy compared to gray-scale only methods, we experimentally applied the proposed RSD scheme to the YCbCr and HSV color spaces derived from the RGB model. In the YCbCr color space, Y denotes the luma component, and Cb and Cr are the blue-difference and red-difference chroma components. In the HSV color space, H denotes the hue component. S and V are the saturation and lightness components, respectively. In general, the V plane in HSV and the Y plane in YCbCr can be regarded as transformed gray images.

Table 3 exhibits the average BER extracted from each individual plane (or layer) drawn from the HSV/YCbCr/RGB color models. The results indicated that the BERs obtained from the R, G, and B-layers were somewhat different but roughly on the same scale. Unlike the situations in the RGB color model, the BERs acquired from the Y, Cb, and Cr were not zero when the attack was absent. This deficiency shall be ascribed to the conversion between the RGB and YCbCr models, which may slightly perturb the pixel values in a color image. In the cases of JPEG and JPEG2000 compression (i.e., A1 and A2), the watermark bits hidden in the Y plane often received better protection. By contrast, the Cb and Cr planes showed better robustness against the lowpass (A5) and unsharp filtering (A6). Overall, for the YCbCr color model, the accuracy of the retrieved watermark pertained not only to the watermarking planes but to the attack types as well.

When applying the proposed RSD to the HSV color space, only the V plane rendered results analogous to that seen in the RGB color model. The watermarks embedded in the H and S planes merely showed limited resistance against all attacks. The cause can be ascribed to the inherent nature of the image file format, which restricts the outputs to be unsigned integers between 0 and 255. Note that the conversion from the HSV model back to the displayable RGB model requires another unsigned integer casting. It is the final data type casting that destroys the watermarks embedded in the HSV model.

V. CONCLUSION

In this paper, level shifting, intentional perturbation, dominance identification, orthonormal reconstruction, distortion compensation and recursive regulation techniques are incorporated into a block-wise Schur decomposition (SD)-based scheme to reinforce blind color image watermarking. The reinforced scheme not only remedies the shortcomings of previous SD-based schemes but also provides a mechanism to ensure an accurate retrieval of the embedded watermark. Moreover, the distortion caused by watermarking can be post-compensated while the embedded information remains intact. Compared with other SD-based watermarking schemes, the proposed RSD exhibits superior robustness and adequate imperceptibility. Computer simulations confirm that the proposed scheme can withstand a variety of image processing attacks. Except for the JPEG compression with low quality factors, the proposed RSD is capable of carrying out effective blind image watermarking at a payload capacity of 1/16 bit per pixel. In future research we will seek to overcome this weakness via the development of a RSD that copes with image blocks of size 8×8 pixels.

REFERENCES

[1] A. M. Eskicioglu and E. J. Delp, "An overview of multimedia content protection in consumer electronics devices," *Signal Process., Image Commun.*, vol. 16, pp. 681–699, Apr. 2001.

[2] O. Jane, E. Elbaşi, and H. G. İlk, "Hybrid non-blind watermarking based on DWT and SVD," *J. Appl. Res. Technol.*, vol. 12, no. 4, pp. 750–761, 2014.
[3] X. Zhu, A. T. S. Ho, and P. Marziliano, "A new semi-fragile image watermarking with robust tampering restoration using irregular sampling," *Signal Process., Image Commun.*, vol. 22, pp. 515–528, Jun. 2007.
[4] P. Tao and A. M. Eskicioglu, "An adaptive method for image recovery in the DFT domain," *J. Multimedia*, vol. 1, no. 6, pp. 36–45, 2006.
[5] T. K. Tsui, X.-P. Zhang, and D. Androutsos, "Color image watermarking using multidimensional Fourier transforms," *IEEE Trans. Inf. Forensic Security*, vol. 3, no. 1, pp. 16–28, Mar. 2008.
[6] X. Kang, J. Huang, Y. Q. Shi, and Y. Lin, "A DWT-DFT composite watermarking scheme robust to both affine transform and JPEG compression," *IEEE Trans. Circuits Syst. Video Technol.*, vol. 13, no. 8, pp. 776–786, Aug. 2003.
[7] H.-T. Hu and L.-Y. Hsu, "A mixed modulation scheme for blind image watermarking," *AEU-Int. J. Electron. Commun.*, vol. 70, pp. 172–178, Feb. 2016.
[8] L.-Y. Hsu and H.-T. Hu, "Robust blind image watermarking using crisscross inter-block prediction in the DCT domain," *J. Vis. Commun. Image Represent.*, vol. 46, pp. 33–47, Jul. 2017.
[9] T. Zong, Y. G. Xiang, S. Guo, and Y. Rong, "Rank-based image watermarking method with high embedding capacity and robustness," *IEEE Access*, vol. 4, pp. 1689–1699, 2016.
[10] F. Ernawan and M. N. Kabir, "A robust image watermarking technique with an optimal DCT-psychovisual threshold," *IEEE Access*, vol. 6, pp. 20464–20480, 2018.
[11] N. A. Loan, N. N. Hurrah, S. A. Parah, J. W. Lee, J. A. Sheikh, and G. M. Bhat, "Secure and robust digital image watermarking using coefficient differencing and chaotic encryption," *IEEE Access*, vol. 6, pp. 19876–19897, 2018.
[12] S. A. Parah, J. A. Sheikh, N. A. Loan, and G. M. Bhat, "Robust and blind watermarking technique in DCT domain using inter-block coefficient differencing," *Digit. Signal Process.*, vol. 53, pp. 11–24, Jun. 2016.
[13] H.-T. Hu and L.-Y. Hsu, "Collective blind image watermarking in DWT-DCT domain with adaptive embedding strength governed by quality metrics," *Multimedia Tools Appl.*, vol. 76, no. 5, pp. 6575–6594, 2016.
[14] S. Ono, T. Maehara, and K. Minami, "Coevolutionary design of a watermark embedding scheme and an extraction algorithm for detecting replicated two-dimensional barcodes," *Appl. Soft Comput.*, vol. 46, pp. 991–1007, Sep. 2016.
[15] Z. Guannan, W. Shuxun, and W. Quan, "An adaptive block-based blind watermarking algorithm," presented at the 7th Int. Conf. Signal Process. (ICSP), 2004.
[16] A. Shehab, M. Elhoseny, K. Muhammad, A. K. Sangaiah, P. Yang, H. Huang, and G. Hou, "Secure and robust fragile watermarking scheme for medical images," *IEEE Access*, vol. 6, pp. 10269–10278, 2018.
[17] T. K. Araghi, A. A. Manaf, and S. K. Araghi, "A secure blind discrete wavelet transform based watermarking scheme using two-level singular value decomposition," *Expert Syst. Appl.*, vol. 112, pp. 208–228, Dec. 2018.
[18] X. Wu and W. Sun, "Robust copyright protection scheme for digital images using overlapping DCT and SVD," *Appl. Soft Comput.*, vol. 13, pp. 1170–1182, Feb. 2013.
[19] C.-C. Chang, P. Tsai, and C.-C. Lin, "SVD-based digital image watermarking scheme," *Pattern Recognit. Lett.*, vol. 26, pp. 1577–1586, Jul. 2005.
[20] P. Rasti, G. Anbarjafari, and H. Demirel, "Colour image watermarking based on wavelet and QR decomposition," in *Proc. 25th Signal Process. Commun. Appl. Conf. (SIU)*, May 2017, pp. 1–4.
[21] Q. Su, G. Wang, X. Zhang, G. Lv, and B. Chen, "An improved color image watermarking algorithm based on QR decomposition," *Multimedia Tools Appl.*, vol. 76, no. 1, pp. 707–729, Jan. 2017.
[22] S. Wang, W. Zhao, and Z. Wang, "A gray scale watermarking algorithm based on LU factorization," in *Proc. Int. Symp. Inf. Process.*, May 2008, pp. 598–602.
[23] Q. Su, G. Wang, X. Zhang, G. Lv, and B. Chen, "A new algorithm of blind color image watermarking based on LU decomposition," *Multidimensional Syst. Signal Process.*, vol. 29, no. 3, pp. 1055–1074, Jul. 2018.
[24] Q. Su and B. Chen, "An improved color image watermarking scheme based on Schur decomposition," *Multimedia Tools Appl.*, vol. 76, pp. 24221–24249, Nov. 2017.
[25] J. Li, C. Yu, B. B. Gupta, and X. Ren, "Color image watermarking scheme based on quaternion Hadamard transform and Schur decomposition," *Multimedia Tools Appl.*, vol. 77, pp. 4545–4561, Feb. 2018.
[26] Q. Su, Y. Niu, X. Liu, and Y. Zhu, "Embedding color watermarks in color images based on Schur decomposition," *Opt. Commun.*, vol. 285, no. 7, pp. 1792–1802, Apr. 2012.
[27] G. H. Golub and C. F. Van Loan, *Matrix Computations*, 3rd ed. Baltimore, MD, USA: The Johns Hopkins Univ. Press, 1996.
[28] L. N. Trefethen and D. Bau, *Numerical Linear Algebra*. Philadelphia, PA, USA: Society for Industrial and Applied Mathematics, 1997.
[29] F. Liu, H. Yang, and Q. Su, "Color image blind watermarking algorithm based on Schur decomposition," *Appl. Res. Comput.*, vol. 34, pp. 3085–3093, Oct. 2017.
[30] Q. Su, Z. Yuan, and D. Liu, "An approximate Schur decomposition-based spatial domain color image watermarking method," *IEEE Access*, vol. 7, pp. 4358–4370, 2019.
[31] Y. Kiani, "Free vibration of FG-CNT reinforced composite spherical shell panels using Gram-Schmidt shape functions," *Compos. Struct.*, vol. 159, pp. 368–381, Jan. 2017.
[32] Å. Björck, "Numerics of Gram-Schmidt orthogonalization," *Linear Algebra Appl.*, vols. 197–198, pp. 297–316, 1994.
[33] CVG. University of Granada. (2014). *CVG-UGR Image Database*. [Online]. Available: http://decsai.ugr.es/cvg/dbimagenes/c512.php
[34] V. I. Arnold and A. Avez, *Ergodic Problems of Classical Mechanics*. New York, NY, USA: Benjamin, 1968.
[35] M. Ahmad and M. S. Alam, "A new algorithm of encryption and decryption of images using chaotic mapping," *Int. J. Comput. Sci. Eng.*, vol. 2, no. 1, pp. 46–50, 2009.
[36] Z. Wang, A. C. Bovik, H. R. Sheikh, and E. P. Simoncelli, "Image quality assessment: From error visibility to structural similarity," *IEEE Trans. Image Process.*, vol. 13, no. 4, pp. 600–612, Apr. 2004.
[37] C.-S. Shieh, H.-C. Huang, F.-H. Wang, and J.-S. Pan, "Genetic watermarking based on transform-domain techniques," *Pattern Recognit.*, vol. 37, pp. 555–565, Mar. 2004.

LING-YUAN HSU received the M.S. degree from National Dong Hwa University, Hualien, Taiwan, in 2004, and the Ph.D. degree from the Department of Computer Science and Information Engineering, National Taiwan University of Science and Technology, Taipei, Taiwan, in 2013. He is currently an Associate Professor with the Department of Information Management, St. Mary's Junior College of Medicine, Nursing and Management, Taiwan. His research interests include artificial intelligence and signal processing.

HWAI-TSU HU received the B.S. degree in electrical engineering from National Cheng Kung University, Taiwan, in 1985, and the M.S. and Ph.D. degrees in electrical engineering from the University of Florida, USA, in 1990 and 1993, respectively. Since 1998, he has been a Professor with the Department of Electronic Engineering, National ILan University, Taiwan. His research interests include speech, audio, and image signal processing.